HHS Public Access

Author manuscript

Nat Immunol. Author manuscript; available in PMC 2014 September 01.

Published in final edited form as:

Nat Immunol. 2014 March ; 15(3): 239–247. doi:10.1038/ni.2823.

The transcription factor DREAM represses A20 and mediates inflammation

Chinnaswamy Tiruppathi[1], **Dheeraj Soni**[1], **Dong-Mei Wang**[1], **Jiaping Xue**[1], **Vandana Singh**[1], **Prabhakar B. Thippegowda**[1], **Bopaiah P. Cheppudira**[1], **Rakesh K. Mishra**[1], **Auditi DebRoy**[1], **Zhijian Qian**[2], **Kurt Bachmaier**[1], **Youyang Zhao**[1], **John W. Christman**[1], **Stephen M. Vogel**[1], **Averil Ma**[3], and **Asrar B. Malik**[1]

[1]Department of Pharmacology and the Center for Lung and Vascular Biology, University of Illinois, Chicago, IL, USA

[2]Department of Hematology/Oncology, College of Medicine, University of Illinois, Chicago, IL, USA

[3]Department of Medicine, School of Medicine, University of California at San Francisco, San Francisco, CA, USA

Abstract

Here we show that the transcription-repressor DREAM binds to the A20 promoter to repress the expression of A20, the deubiquitinase suppressing inflammatory NF-κB signaling. DREAM-deficient (*Dream*$^{-/-}$) mice displayed persistent and unchecked A20 expression in response to endotoxin. DREAM functioned by transcriptionally repressing A20 through binding to downstream regulatory elements (DREs). In contrast, USF1 binding to the DRE-associated E-box domain activated A20 expression in response to inflammatory stimuli. These studies define the critical opposing functions of DREAM and USF1 in inhibiting and inducing A20 expression, respectively, and thereby the strength of NF-κB signaling. Targeting of DREAM to induce USF1-mediated A20 expression is therefore a potential anti-inflammatory strategy in diseases such as acute lung injury associated with unconstrained NF-κB activity.

The transcriptional repressor downstream regulatory element antagonist modulator (DREAM) is a Ca^{2+}-binding protein family member containing 4 Ca^{2+} binding motifs ("EF-hands") that interact as a tetramer with downstream regulatory element (DRE) to inhibit transcription[1]. Ca^{2+} signaling has been linked to DREAM activation because decreased intracellular Ca^{2+} concentration increases the binding affinity of DREAM to DRE, and thereby to repress transcriptionally the target genes[1]. DREAM binding to DRE was reversed

---

Address for correspondence: Chinnaswamy Tiruppathi, Department of Pharmacology (M/C868), College of Medicine, University of Illinois, 835 South Wolcott Ave, Chicago, IL 60612; Telephone # 312-355-0249; Fax # 312-996-1225; tiruc@uic.edu.

AUTHORS CONTRIBUTIONS:

C.T., D.S., J.W.C., A.M. and A.B.M. designed the research; C.T., D.S., D.W., J.X., V.S., P.B.T., B.P.C., R.K.M., A.D., Z. Q., K.B., Y.Z., and S. M.V. did the experiments; C.T. analyzed data; C.T. and A.B.M wrote the manuscript.

COMPETEING FINANCIAL INTERESTS:

The authors declare no competing financial interests.

by cAMP activation of protein kinase A (PKA) through phosphorylation of the DREAM-interacting protein α-CREM, which blocked the binding of DREAM to DRE[2,3]. DREAM is involved in sensing pain[4,5], a hallmark of inflammation. DREAM is expressed in pain sensing areas of the spinal cord in association with κ-opiate receptors[4,5] but it is also present in immune cells such as T and B lymphocytes[6,7] where its function is not understood. Transgenic mice expressing a dominant-active DREAM mutant showed markedly reduced production of the cytokines IL-2, IL-4, and IFN-γ, increased B cell numbers, and decreased IgG production[6,7]. As activation of the transcription factor NF-κB may regulate some of these responses, we surmised that DREAM is involved in the mechanism of inflammation through its ability to control NF-κB signaling. In addition to the transcription repressor function of DREAM, the transcription factor upstream stimulatory factor 1 (USF1), which binds to the E-box domain associated with DREs on the A20 promoter, is also involved in A20 (TNFAIP3) gene transcription initiation[8]. An important question therefore arises whether DREAM and USF1 function cooperatively to coordinate A20 transcription, and thus the magnitude of pro-inflammatory NF-κB signaling.

NF-κB is composed of dimers of 5 proteins, p50, p52, p65 (RelA), RelB and c-Rel, that exist in inactive form in the cytoplasm bound to 3 inhibitory proteins, IκBα, IκBβ and IκBε[9–11]. Activation of NF-κB in the classical pathway requires activation of IκB-kinase (IKK) complex, containing the kinases IKKα and IKKβ and the regulatory protein IKKγ[9]. Activated IKKs phosphorylate IκBα and IκBβ, which leads to their proteolytic degradation and frees NF-κB dimer to translocate to the nucleus to induce expression of multiple target genes. Signaling via Toll-like receptors (TLRs), interleukin-1 receptor (IL-1R), tumor necrosis factor receptor (TNFR), and G protein-coupled receptors all induce activation of IKK resulting in NF-κB activity[9–12]. The identification of feedback checks on NF-κB activation has been of great interest as possible drug targets. A key downregulator of NF-κB is the deubiquitinase A20[13], first identified as an anti-apoptotic protein in human umbilical vein endothelial cells (HUVECs)[14]. NF-κB within hours of activation in response to TNF or LPS induced A20 expression[15–17]. A20 in turn inhibited the functions of TNF receptor-associated factors 2, 5, and 6 (TRAF2, TRAF5, TRAF6), receptor interacting proteins 1 and 2 (RIP1 and RIP2), and IKKγ upstream of IKKs by editing ubiquitin chains on these proteins essential for IKK activation[15–21]. The ovarian tumor (OTU) domain of A20 mediates deubiquitylation of K63-linked polyubquitylated proteins and C-terminal zinc finger domain of A20 possesses ubiquitin ligase activity, which mediates K48-linked polyubiquitylation of target proteins to induce its proteasomal degradation and terminate NF-κB signaling[19,20]. *Tnfaip3* (A20)-deficient mice displayed spontaneous inflammation and cachexia and died prematurely[22]. Targeted cardiac over-expression of A20 improved outcomes by suppressing inflammation in the mouse model of myocardial infarction[23]. A20 over-expression was also protective in the atherosclerosis mouse model whereas A20 haplo-insufficiency resulted in severe atherosclerosis[24]. These studies underscore the importance of A20 in restricting inflammation. However, the transcriptional mechanisms of A20 expression are poorly understood. Therefore, to gain insight into the transcriptional mechanisms of A20 expression, we analyzed the A20 promoter and observed the presence of DREAM binding DRE elements both upstream and downstream of the transcription start site (TSS) in intron-1 of human and mouse A20 genes. In addition, the E-box domain was

shown to be an integral component of DREs. Further, we observed that both basal and endotoxin-induced A20 expression in endothelial cells and macrophages was markedly augmented in *Kcnip3*$^{-/-}$ (hereafter referred to as *Dream*$^{-/-}$) mice, which in turn prevented the activation of NF-κB signaling. Production of inflammatory cytokines IL-6, MCP-1, and TNF, lung neutrophil (PMN) sequestration, and ICAM-1 expression were also suppressed in response to endotoxin and survival in *Dream*$^{-/-}$ mice was greatly enhanced compared to wild type.

RESULTS

DREAM mediates inflammatory lung injury and mortality

We first determined the expression of ICAM-1, pathological changes in lungs, and lung myeloperoxidase (MPO) activity (an indicator of PMN sequestration) at different times in wild-type (WT) and *Dream*$^{-/-}$ mice after i.p. lipopolysaccharide (LPS, 10 mg/kg). LPS induced severe lung injury and sequestration of PMNs in lungs and increased ICAM-1 protein expression in a time-dependent manner, whereas these responses were significantly reduced in *Dream*$^{-/-}$ mouse lungs (Fig. 1a–c). To quantify changes in lung vascular permeability, an index of inflammatory injury, we measured pulmonary microvessel filtration coefficient ($K_{f,c}$). LPS significantly increased $K_{f,c}$ in WT lungs whereas DREAM deletion abrogated the response (Fig. 1d). We also observed marked reduction in the number of PMNs and MPO activity in bronchoalveloar lavage fluid (BALF) from *Dream*$^{-/-}$ mice compared with WT (Fig. 1e). In addition, BALF concentrations of pro-inflammatory mediators IL-6, MCP-1, and TNF from *Dream*$^{-/-}$ mice in response to LPS were reduced compared with WT (Fig. 1f). In survival studies, 90% of WT mice died within 6 days of LPS administration whereas only 50% of *Dream*$^{-/-}$ mice died during the same period, and thereafter there were no further deaths (Fig. 1g). To validate the above findings in a severe model of sepsis, we used cecal ligation and puncture (CLP) to induce polymicrobial sepsis in age, sex, and weight matched WT and *Dream*$^{-/-}$ mice. In these studies, 100% mortality was seen in WT mice within 36 h of CLP whereas only 20% of *Dream*$^{-/-}$ mice died within the same period (Fig. 1h); 50% of *Dream*$^{-/-}$ mice were alive 3 days after CLP and 40% remained alive more than 2 weeks after CLP (Fig. 1h).

To determine whether DREAM deficiency in hematopoietic cells as opposed to non-hematopoietic cells such as endothelial cells (which comprise ~50% of the total lung cell population[25]) and epithelial cells was responsible for its anti-inflammatory function uncovered in *Dream*$^{-/-}$ mice, we transplanted WT-mouse bone marrow (BM) cells into lethally irradiated *Dream*$^{-/-}$ mice[26]. These chimeric (WT-BM→*Dream*$^{-/-}$) mice were used for experiments 6 weeks after transplantation. Male specific *Sry* gene analysis using DNA isolated from recipient mice blood cells showed highly efficient reconstitution of WT bone marrow (Supplemental Fig. 1a). On challenging WT, *Dream*$^{-/-}$, or WT-BM→*Dream*$^{-/-}$ mice similarly with LPS, we observed that PMN sequestration in lungs, presence of chemokines and cytokines (MCP-1, IL-6, and TNF) in BALF, and expression of ICAM-1 in lungs of WT-BM→*Dream*$^{-/-}$ mice were not significantly different from *Dream*$^{-/-}$ mice (Supplemental Fig. 1b–d,f). Serum concentrations of MCP-1, IL-6 and TNF after LPS challenge in WT-BM→*Dream*$^{-/-}$ mice were not significantly different from WT mice

(Supplemental Fig. 1e). However, serum MCP-1 concentration did not increase after LPS in *Dream*$^{-/-}$ mice relative to WT mice (Supplemental Fig. 1e), suggesting that unlike the changes in serum concentrations of IL-6, and TNF the primary source of MCP-1 is hematopoietic cells; this finding is consistent with MCP-1 as being primarily generated by hematopoietic cells[27]. Mortality in WT-BM →*Dream*$^{-/-}$ mice resembled that of *Dream*$^{-/-}$ mice (Supplemental Fig. 1f). These results together suggest that DREAM signaling in hematopoietic cells was not responsible for the full-blown inflammatory lung injury response.

DREAM and USF1 coordinate A20 transcription

We observed that LPS-induced inflammatory responses were attenuated in *Dream*$^{-/-}$ mice; however, the mechanism for the attenuation of inflammation in *Dream*$^{-/-}$ mice is unknown. Since DREAM represses target genes by binding to DRE elements, we asked whether DREAM represses the anti-inflammatory deubiquitnase A20 resulting in inflammation. Thus, we analyzed the 5′-regulatory region of the h*A20* gene and identified the presence of DREAM binding "DRE" (GTCA sequence) sites downstream of the TSS in intron-1 and 3 additional DRE sites upstream of TSS (Fig. 2a). one of these sites, DRE3, had an overlapping E-box sequence (Fig. 2a).

Using chromatin immunoprecipitation (ChIP) to determine DREAM binding to DREs of A20 promoter in human lung microvessel endothelial cells (HLMVECs), we observed that basal binding of DREAM to DRE3 and DRE4 in h*A20* promoter was significantly elevated (Fig. 2b–e) consistent with DREAM's transcription repressing function. In contrast to DREAM binding to DRE3 and DRE4, DREAM did not bind to DRE1 and DRE2. LPS or TNF challenge induced uncoupling of DREAM from DRE3 and DRE4, which persisted for 90 min, but DREAM binding cycled back within 180 min (Fig. 2d,e), indicating a reversible event. Thus, DREAM's function in transcriptionally suppressing *h*A20 expression involves reduction in binding of DREAM to DRE3 and DRE4 followed by time-dependent restored binding to the same domain.

Next to address the possible coordinating role of the overlapping E-box sequence associated with DRE3 in regulating A20 transcription (Fig. 2a), we studied the transcription factor USF1, the dominant E-box binding protein involved in A20 gene transcription initiation[8]. USF1 binding to DRE3-E-box increased within 90 min in response to LPS or TNF (this increase was opposite to the reduced DREAM binding during this period), and as with DREAM binding, USF1 binding returned to baseline within 120 after stimulation (Fig. 2f). To investigate whether USF1 was essential for regulating A20 transcription[8], we next silenced USF1 expression in HUVECs and measured A20 expression. USF1 knockdown prevented TNF-induced A20 expression (Fig. 2g). These results show that DREAM functioned basally to repress A20 transcription, but in response to inflammatory stimuli DREAM dissociated from DRE, and USF1 bound to DRE3-E-box to signal A20 transcription.

To address whether DREAM also represses the mouse *A20* (*Tnfaip3*) gene, we analyzed m*A20* promoter sequence and observed that *m*A20 promoter had "DRE" site downstream of TSS in intron-1 and 2 additional DRE sites upstream of TSS (Fig. 3a). Similar to *h*A20 gene,

the *m*A20 gene DRE2 has an overlapping E-box sequence (Fig. 3a). We observed that basally DREAM bound primarily to the DRE3 domain of *m*A20 promoter, and to a lesser extent to DRE2 (Fig. 3b–d). As expected DREAM binding was not seen in *Dream*$^{-/-}$ cells (Fig. 3b–d). DREAM binding to DRE2 and DRE3 decreased upon LPS challenge in a time-dependent manner in WT-macrophages as in the human cells above, and returned to baseline by 90 min (Fig. 3c,d). We also observed a positive correlation between the amount of DREAM protein in the nucleus and DREAM binding to the DREs (Supplemental Fig. 2A). Since DRE2 in the *m*A20 promoter overlaps with E-box, we determined interaction between DRE2-E-box and USF1. USF1 binding to DRE2-E-box increased maximally within 90 min after LPS challenge (Fig. 3e) similar to results above in human cells showing temporal USF1 binding to *h*DRE3-E-box (Fig. 2f). USF1 binding to DRE2-E-box was seen basally in *Dream*$^{-/-}$ macrophages (Fig. 3e) indicating a role of USF1 binding in mediating the persistent A20 transcription in the absence of the repressive effect of DREAM. USF1 binding to DRE-E-box increased in *Dream*$^{-/-}$ macrophages until peaking at 90 min post-LPS to the same level as in WT cells (Fig. 3e), indicating USF1 continued to bind to the A20 promoter in the absence of DREAM binding. These findings collectively demonstrate that similar to *h*A20, DREAM represses *m*A20 transcription by binding to DRE elements whereas USF1 binding to the DRE-associated E-Box domain in response to inflammatory stimuli promotes *m*A20 transcription. Thus, these results analyzing the A20 promoter describe a model for the regulation of A20 transcription by the coordinated actions of DREAM and USF1 (Supplemental Fig. 2B).

DREAM modulates A20 expression in inflammation

We observed that DREAM protein was expressed in variety of cells involved in inflammation, including lung endothelial cells (LECs), PMNs, and bone marrow derived macrophages (BMDMs) of mice (Fig. 4a–c). There was ~3-fold increased expression of A20 protein in LECs, PMNs, and BMDMs from *Dream*$^{-/-}$ mice compared with WT mice (Fig. 4a–c) consistent with DREAM's role in suppressing A20 transcription in these cells (as described in Fig. 2 and Fig. 3). Since LPS-induced acute lung injury was markedly reduced in *Dream*$^{-/-}$ (Fig. 1), we next investigated the possibility that augmented A20 expression in these mice was responsible for the reduced lung injury response. LPS challenge induced 3–4 fold greater A20 protein expression in lungs of *Dream*$^{-/-}$ mice compared to WT (Fig. 4d). It was shown previously that DREAM represses c-Fos expression by binding to DRE element in the *Fos* promoter[1]. As a positive control, we determined LPS induced c-Fos expression in WT and *Dream*$^{-/-}$ mice. We observed that c-Fos protein expression in response to LPS was increased in lungs of *Dream*$^{-/-}$ mice compared to WT mice (Supplemental Fig. 3), indicating that DREAM deficiency augments the expression of DREAM target genes.

A20 knockdown restores inflammation in *Dream*$^{-/-}$ mice

To address the causal role of augmented A20 expression seen in *Dream*$^{-/-}$ mice (Fig. 4a–c) in mediating the markedly reduced inflammatory lung injury response (described in Fig. 1), we silenced A20 expression in lung vascular endothelial cells *in vivo* using a liposome-mediated delivery, which targets lung endothelial cells[28,29], of small interference RNA (siRNA). Here we studied DREAM signaling in endothelial cells since DREAM's role in these cells was shown to be essential for inflammatory lung injury (Supplemental Fig. 1). At

48 h after siRNA delivery, we observed >80% reduction in A20 protein in A20-siRNA injected *Dream*$^{-/-}$ mice compared to control *Dream*$^{-/-}$ mice or control-siRNA (Sc-siRNA) injected *Dream*$^{-/-}$ mice (Fig. 4e). ICAM-1 expression induced by LPS challenge of A20-siRNA treated *Dream*$^{-/-}$ mice was significantly increased compared to control *Dream*$^{-/-}$ mice or Sc-siRNA-treated *Dream*$^{-/-}$ mice (Fig. 4f,g). Also PMN sequestration (assessed by MPO activity) was increased in lungs of A20-siRNA treated *Dream*$^{-/-}$ mice compared with control *Dream*$^{-/-}$ mice or Sc-siRNA treated *Dream*$^{-/-}$ mice (Fig. 4h). Thus, the upregulated A20 expression in lung endothelial cells seen in *Dream*$^{-/-}$ mice was required for mitigating inflammatory lung injury.

DREAM promotes TAK1-mediated NF-κB activation

We next addressed the mechanisms by which the DREAM-induced inhibition of A20 expression mediated inflammatory lung injury. As A20 cleaves K63-linked polyubiquitin chains in TRAF2 and TRAF6 to prevent TAK1 kinase activity[15–21], and the subsequent activation of NF-κB[15–21], we focused on TNF-induced activation of both TAK1 and downstream IKK in LECs obtained from WT and *Dream*$^{-/-}$ mice. We observed time-dependent TNF-induced phosphorylation of IKKβ in WT-LECs, but this effect was suppressed in *Dream*$^{-/-}$-LECs (Fig. 5a). We next investigated the role of DREAM in mediating expression of IκBα based on the concept that NF-κB signaling is required for IκBα expression, and IκBα in a negative feedback manner inhibits NF-κB activation[9,10]. We observed that basal expression of IκBα was significantly reduced in LECs from *Dream*$^{-/-}$ mice compared to WT mice (Fig. 5b). TNF challenge produced time-dependent increases in IκBα transcript (Fig. 5c) and protein (Fig. 5b) in WT-LECs. These responses were abrogated in *Dream*$^{-/-}$-LECs (Fig. 5b,c). To address whether TAK1 activation was also suppressed in *Dream*$^{-/-}$-LECs, we treated LECs from WT and *Dream*$^{-/-}$ mice with TNF, and measured phosphorylation of TAK1[30]. Here we observed time-dependent phosphorylation of TAK1 in WT-LECs but not in *Dream*$^{-/-}$-LECs in response to TNF (Fig. 5d). To determine whether the suppressed activation of IKK in *Dream*$^{-/-}$-LECs was the result of enhanced A20 expression *per se*, we performed a rescue experiment in which WT-DREAM or mut-DREAM (unable to bind DNA) was expressed in *Dream*$^{-/-}$-LECs. We observed that expression of WT-DREAM, but not of mut-DREAM, in *Dream*$^{-/-}$-LECs restored IKK activation in response to TNF (Fig. 5e).

Since TAK1 lies upstream of JNK and p38 signaling[30], we validated the role of DREAM in regulating TAK1 activation by also assessing the MAP kinases JNK and p38 activation. TNF-induced phosphorylation of both JNK and p38 was markedly reduced in LECs from *Dream*$^{-/-}$ mice compared with WT mice (Fig. 6a,b). To address whether reduced phosphorylation of these kinases was the result of increased A20 expression seen in *Dream*$^{-/-}$ mice, we silenced A20 and measured TNF-induced phosphorylation of p38. Here TNF-induced p38 phosphorylation was restored in A20 knockdown in *Dream*$^{-/-}$ LECs (Fig. 6c). In further support of these findings, we observed markedly reduced transcript expression of MCP-1 and ICAM-1 in *Dream*$^{-/-}$ LECs in response to TNF challenge (Fig. 6d); in contrast, A20 expression was augmented in *Dream*$^{-/-}$ LECs (Fig. 6e).

Next we studied the role of DREAM in regulating endotoxin-induced NF-κB signaling. A20 protein expression was increased to a greater extent in bone marrow-derived macrophages (BMDMs) from *Dream*$^{-/-}$ mice compared to WT (Fig. 6f). To address the functional relevance of enhanced A20 expression in the endotoxin response, we studied activation of TAK1 and IKK in macrophages from *Dream*$^{-/-}$ and WT mice following LPS challenge. As in the above studies, the LPS-induced activation of TAK1 and IKK were both markedly reduced and delayed in *Dream*$^{-/-}$ cells compared with WT (Supplemental Fig. 4a,b). These results support the notion that augmented A20 expression restricts TAK1-mediated IKK and MAPK activation in *Dream*$^{-/-}$ cells.

DREAM regulates A20 targets mediating NF-κB signaling

We then set out to determine the consequence of DREAM-induced downregulation of A20 in mediating activation of NF-κB (as shown in Fig. 1). For this, we evaluated the expression of A20 targets in lungs of *Dream*$^{-/-}$ and WT mice. Expression of TRAFs (TRAF2 and TRAF6) (Fig. 7a), RIPs (RIP1 and RIP2) (Fig. 7a), IκBα (Fig. 7a), and IKKγ (Fig. 7b) were suppressed in *Dream*$^{-/-}$ mouse lungs compared to WT. IKKα and IKKβ were however unaffected (Fig. 7b). Next we determined the expression of NF-κB proteins in lungs of *Dream*$^{-/-}$ and WT mice. p65-RelA expression was not different between *Dream*$^{-/-}$ and WT mouse lungs (Fig. 7c), whereas NF-κB1, NF-κB2, RelB, and c-Rel protein expression was suppressed (Fig. 7c). Also the expression levels of RIPs, TRAFs, IKKγ, IκBα, and NF-κB proteins (NF-κB1, NF-κB2, RelB, and c-Rel) were reduced in *Dream*$^{-/-}$-LECs compared to WT-LECs (Fig. 7d). Next, we measured mRNA expression of these NF-κB signaling components by qRT-PCR. Expression of mRNA for RIP2 and TRAF2 was significantly reduced in lungs of *Dream*$^{-/-}$ mice (Supplemental Fig. 5), whereas mRNA expression of RIP1, TRAF6, NEMO, NF-κB1, NF-κB2, RelB, and c-Rel was not altered in lungs of *Dream*$^{-/-}$ mice compared to WT mice (Supplemental Fig. 5).

To address whether decreased expression of NF-κB signaling components seen in *Dream*$^{-/-}$ mice is the result of A20, we performed rescue experiments in which WT-DREAM or DNA-binding defective mutant DREAM (mut-DREAM) was ectopically expressed in LECs of *Dream*$^{-/-}$ mice. In this study, WT-DREAM but not mut-DREAM expression suppressed A20 as well as c-Fos (another DREAM regulated protein[1]) expression in *Dream*$^{-/-}$-LECs (Fig. 8). Expression of WT-DREAM (but not mut-DREAM) restored the expression of A20 targets and NF-κB signaling components except RIP2 in LECs of *Dream*$^{-/-}$ mice (Fig. 8). These findings together demonstrate that DREAM-mediated suppression of A20 expression was responsible for activating NF-κB signaling and the NF-κB target genes responsible for inflammatory lung injury. Based on the present results, we propose a model (Supplemental Fig. 6) for the mechanism of DREAM regulation of A20 expression and thereby the inflammatory NF-κB signaling pathways.

DISCUSSION

The present results demonstrate the crucial pro-inflammatory function of the transcription repressor DREAM and its interaction with the transcription activator USF1 in the mechanism of A20 expression and the subsequent tuning of NF-κB activity. DREAM has

been shown to be important in the spinal cord in mediating the sensation of pain[4,5]. Mice lacking DREAM (*Dream*$^{-/-}$) had increased prodynorphin mRNA and dynorphin A peptides in the spinal cord and reduced pain sensation[4]. Here we demonstrated that *Dream*$^{-/-}$ mice failed to develop inflammatory lung injury in response to sepsis as the result of USF1-mediated expression of the deubiquitinase A20, and thereby the downstream inhibition of TAK1-mediated NF-κB activity and signaling.

DREAM was shown to bind constitutively to DRE3 and DRE4 in the h*A20* promoter. DREAM binding decreased for 90 min on LPS or TNF exposure, but returned to baseline within 180 min. The cyclic nature of the DREAM binding response was mirrored by binding of the A20 transcription activator USF1 to the DRE3-E-box; that is, USF1 binding functioned to induce A20 transcription. A similar pattern emerged in the m*A20* promoter, suggesting a well conserved mechanism of coordinated DREAM-USF1 regulation of A20 transcription. The reciprocal function of DREAM and USF1 in regulating A20 expression is consistent with the notion that USF1 binding to the E-box sequence on the A20 promoter is important for mediating A20 gene transcription initiation[8].

We observed in *Dream*$^{-/-}$ mice, in which USF1 binding to the A20 promoter remained intact, that endotoxin resulted in reduced ICAM-1 expression and PMN sequestration in lungs and normal lung vascular barrier function as compared to WT mice. The DREAM-deleted mice also showed markedly reduced generation of NF-κB-transcribed pro-inflammatory mediators IL-6, MCP-1, and TNF and displayed enhanced survival in a CLP model of severe polymicrobial sepsis, results consistent with augmented A20 expression and decreased NF-κB activation in these mice. Therefore, inactivation of DREAM signaling had an indispensible anti-inflammatory function.

As DREAM expressed in hematopoietic[6,7] as well as endothelial cells may be essential in the mechanism of inflammatory lung injury, we addressed whether DREAM deficiency was responsible for DREAM's pro-inflammatory role uncovered in *Dream*$^{-/-}$ mice. In chimeric mice in which WT-mice bone marrow cells were transplanted into *Dream*$^{-/-}$ mice, we observed that PMN sequestration in lungs, lung production of MCP-1, IL-6, and TNF and lung vascular ICAM-1 expression were similar to *Dream*$^{-/-}$ mice. These findings rule out the primary role of DREAM expression in hematopoietic cells in the mechanism of the inflammatory lung injury response. They are however consistent with results showing that selective expression of the degradation-resistant form of NF-κB in the vascular endothelium prevented inflammation in mice[31]. Our results suggest that DREAM's pro-inflammatory role identified in *Dream*$^{-/-}$ mice is likely the result of endothelial cell-expressed DREAM.

Since inflammatory lung injury was markedly reduced in *Dream*$^{-/-}$ mice, we investigated whether the augmented A20 expression was responsible for mediating the response. We silenced A20 expression in lung vascular endothelial cells using liposome-mediated delivery of A20-siRNA[28,29]. ICAM-1 expression and lung PMN sequestration induced by LPS challenge of A20-siRNA treated *Dream*$^{-/-}$ mice were significantly increased compared to control *Dream*$^{-/-}$ mice. Thus, A20 expression in LECs of *Dream*$^{-/-}$ mice was required and sufficient to re-establish the inflammatory lung injury response in these mice.

Based on studies using LECs from *Dream*$^{-/-}$ mice, we demonstrated that the persistent A20 expression in these mice interfered with phosphorylation of TAK1, and thereby downstream activation of IKKβ and NF-κB. To test the functional relevance of this finding, we carried out a crucial rescue experiment in which WT-DREAM or mut-DREAM (unable to bind DRE) was expressed in *Dream*$^{-/-}$ -LECs. In this study, expression of WT-DREAM, but not of mut-DREAM, in *Dream*$^{-/-}$ cells restored IKK activation in response to TNF. These studies demonstrate a key role of DREAM and its relationship with USF1 described above in regulating the activation of TAK1-mediated NF-κB signaling.

Because DREAM and USF1 function through modulating A20 expression, we also determined expression of multiple constituents of the NF-κB signaling pathway that as a consequence might be altered by A20 expression. We observed that expression of p65/RelA, IKKα, and IKKβ was similar between WT and *Dream*$^{-/-}$ mice. A likely explanation of this finding is that these factors are not transcriptionally regulated by NF-κB[32]. We found however that the expression of other NF-κB signaling components TRAFs (TRAF2 and TRAF6), RIPs (RIP1 and RIP2), IκBα, IKKγ, NF-κB1, NF-κB2, RelB, c-Rel were all downregulated in *Dream*$^{-/-}$ mice. mRNA expression of TRAF2 and RIP2 was significantly reduced in *Dream*$^{-/-}$ mice compared with WT mice. Until now transcription mechanisms of TRAF2 expression have not been identified. Our promoter analysis revealed the presence of multiple binding sites for the transcription factor AP1 in both human and mouse TRAF2 genes. It is known that NF-κB signaling mediates transcription of both the human and mouse RIP2 genes[33]. A20 restricts the activation of IKK and MAPK (MAPK signaling is essential for AP1 activation[34]) by blocking TAK1 function[15–21]; therefore, the enhanced A20 expression seen in *Dream*$^{-/-}$ cells likely prevented transcription of TRAF2 and RIP2 by this mechanism. A20 activity also decreased the expression of NF-κB signaling components through proteosomal pathway, which involves A20-mediated deubiquitylation of K63-linked ubiquitin chains followed by ubiquitylation of K48-linked ubiquitin chains on the target molecules[20]. Thus, it is possible that decreased expression of NF-κB signaling components such as TRAF6 and RIP1 may be the result of constitutive A20-mediated proteosomal degradation of these molecules in *Dream*$^{-/-}$ cells. Our findings collectively support a key role of enhanced A20 expression mediated by USF1 in *Dream*$^{-/-}$ mice in inhibiting TAK1-mediated signaling. These findings suggest that the reciprocal relationship between DREAM and USF1 functions as a rheostat regulating A20 expression, and thus enables fine-tuning of NF-κB signaling. The anti-inflammatory function of DREAM deletion described here suggests that targeting DREAM is a potentially useful therapeutic strategy in inflammatory diseases such as acute lung injury.

ONLINE METHODS

Antibodies and other reagents

Polyclonal antibodies generated against DREAM, ICAM-1, USF1, TRAF2, TRAF6, NF-κB1, NF-κB2, RelB, c-Rel, and IκBα were obtained from Santa Cruz Biotechnology, Inc. Anti-A20 mouse monoclonal antibody (mAb; 59A426) was from Calbiochem. c-Fos polyclonal antibody (pAb), phospho-TAK1 (Thr184/187) pAb, TAK1 rabbit mAb (D94D7), phospho-p38 MAPK (Thr/Tyr182) mAb (28B10), p38 MAPK pAb, phospho-SAPK/JNK

(Thr183/Tyr185) rabbit mAb (81E11), SAPK/JNK rabbit mAb (56G8), IKKα pAb, phospho-IKKα/β (Ser176/180) pAb, IKKβ pAb, phospho-IκBα (Ser32) rabbit mAb (14D4), RIP1 pAb, and RIP2 pAb were from Cell Signaling. IKKγ mAb (clone 72C627) and DREAM mAb (clone 40A5) were obtained from Upstate. p65/RelA pAb was from Chemicon. Control siRNA was from Qiagen and *h*USF1-siRNA (SMARTpool, cat # L003617) was from Dharmacon. siRNA transfection reagent was obtained from Santa Cruz Biotechnology, Inc. Lipids (dimethyldioctadecylammonium bromide and chlolesterol) for liposome preparation and anti-β-actin mAb (clone AC-15) were purchased from Sigma. PCR primers were custom-synthesized from Integrated DNA Technologies.

Mice

DREAM knockout (*Dream*$^{-/-}$) mice[4] generated using C57BL/6 background strain was obtained from Dr. Josef Penninger's laboratory (Vienna, Austria). *Dream*$^{-/-}$ mice were backcrossed into a C57BL/6J background for 8 generations. Age matched *Dream*$^{+/+}$ (WT) and *Dream*$^{-/-}$ mice littermates were used for all experiments. All mice were housed in the University of Illinois Animal Care Facility in accordance with institutional guidelines and guidelines of the US National Institute of Health. Veterinary care of these animals and related animal experiments was approved by the University of Illinois Animal Resources Center.

Generation of bone marrow chimeras

Lethal irradiation of *Dream*$^{-/-}$ mice was performed as described[26]. At 3 h following irradiation, mice were transplanted with 1×10^7 isolated *Dream*$^{+/+}$ (WT) bone marrow cells through tail-vein injection[26]. The bone marrow reconstitution was assessed at 3 weeks after transplantation by *Sry* (male specific) gene presence in recipient mice blood cells by qualitative PCR[35]. Mice were used for experiments 6 weeks after bone marrow transplantation.

Lung injury in mice

Age- and weight-matched *Dream*$^{+/+}$ (WT) and *Dream*$^{-/-}$ mice received a single dose (10 mg/kg) of LPS (ultrapure *E. coli* 0111:B4, InvivoGen) intraperitoneally. For histology, 5-μm paraffin-embedded sections prepared from the lungs were stained with hematoxylin and eosin. For MPO assay, lungs were perfused with PBS to remove all blood then used to measure MPO activity[36]. Lung microvascular permeability $K_{f,c}$ was measured using isolated lung preparations as described[37,38]. BALF collection and the inflammatory cells in the BALF were measured as described[39]. Cytokines in the BALF and serum were measured by ELISA (eBioscience). Polymicrobial sepsis was induced by CLP using a 18-gauge needle as described[40]. For survival studies, mice were monitored 4 times daily up to 2 days and then twice daily for two weeks.

In vivo A20 knockdown in mice

*m*A20 target SMARTpool siRNA (Target sequences: AGAGACAUGCCUCGAACUA; GCUGUGAAGAUACGAGAGA; UGUUACUGCCUCUGCGAA; GCACCUAAGCCAACGAGUA) was from Dharmacon. Control siRNA (Sc-siRNA; target

sequence:CAGGGTATCGACGATTACAAA) was obtained from Qiagen. Cationic liposome was prepared using dimethyldioctadecylammonium bromide and chlolesterol (1:1 molar ratio) as we described[28,29]. The liposome and siRNA (Sc-siRNA or A20 target SMARTpool siRNA) was mixed (lipid 8 moles:1 μg siRNA) and the mixture (1 mg siRNA/kg body weight) was intravenously (i.v.) injected in mice[28,29]. At 48 after siRNA delivery, the animals were used for experiments.

Endothelial cells and BMDMs

LECs from age-matched wild type (WT) and *Dream*$^{-/-}$ mice were isolated using anti-platelet endothelial cell adhesion molecule (PECAM)-1 mAb[38]. After isolation the cells were placed in culture and again affinity purified using anti-ICAM-2 mAb. LECs were characterized by their cobblestone morphology, Dil-Ac-LDL uptake, and VE-cadherin expression[38]. Human vascular endothelial cells from umbilical vein and lung microvessel were grown as described by us[12,41]. BMDMs from WT and *Dream*$^{-/-}$ mice were generated by culture of bone marrow cells as described previously[16].

Immunoblotting

Lungs harvested were homogenized in lysis buffer (50 mM Tris-HCl, pH 7.5, 150 mM NaCl, 1 mM EGTA, 1% Triton X-100, 0.25% sodium deoxycholate, 0.1% SDS, and protease inhibitor mixture). The homogenate was centrifuged (14,000g at 4°C for 10 min) and clear supernatant was used for immunoblot. BMDMs stimulated with LPS or endothelial cells stimulated with TNF were lysed with lysis buffer containing phosphatase inhibitor mixture[12]. The lysate was centrifuged and clear supernatant was used for immunoblot[12].

Promoter analysis

Consensus binding sites for transcription factors and repressor elements in the human and mouse A20 genes 5′-regulatory region and intron-1 were analyzed using Genomatix Software (Germany).

ChIP assay

CHIP assay was performed as described[42]. The CHIP-PCR primers used are: *h*A20 DRE1 forward 5′-GTCCATGGAGCGTCGCC-3′, reverse 5′-GGGTCGCTGCCCAACAT-3′; *h*DRE2, forward 5′-GTCTGGGTTTTGAAGTGCTGG-3′, reverse 5′-TGCAACGCTTGGCTCCAAAA-3′; *h*A20 DRE3, forward 5′-CCCGGGGCGGGGCGAGGGAGTTTCTC-3′, reverse 5′-ACTTTCCAAAGTCACGTGACTCTCTGGGTC-3′; *h*A20 DRE4, forward, 5′-GCTGGGAGTTGAGGTCACTGCTGCAGAGGT, reverse 5′-CTTCTGCAAGGTCTACGTGG-3′; *m*A20 DRE1, forward, 5′-TGCACTGCATCCAACCTGAA-3′, reverse 5′-AAATCGCGGTGATGGGAACT-3′; *m*A20 DRE2, forward, 5′-GTTCCCATCACCGCGATTTC-3′, reverse, 5′-GGAGCATCGCTCACCTCTTG-3′; *m*A20 DRE3, forward, 5′-AGAGGTGAGCGATGCTCCG-3′, reverse, 5′-CGACCACACGACCTAGGAAC-3′. The relative sample DNA-protein interaction was calculated with the following formula: $2^{\Delta Ctx}-2^{\Delta Ctb}$, where ΔCtx = Ct input − Ct sample and ΔCtb = Ct input − Ct control Ab.

Quantitative real-time PCR (QRT-PCR)

Total RNA from lung tissue or LECs was isolated and reverse-transcribed (RT) using oligo-dt primers with SuperScript reverse transcriptase (Invitrogen). The obtained cDNA was mixed with SYBR Green PCR Master mix (AB Applied biosystems) and gene specific primers for PCR. The quantitative PCR was carried out utilizing ABI Prism 7000. GAPDH expression was used as internal control. The following primers were used: *m*IκBα: forward (F): 5′-AACCTGCAGCAGACTCCAC-3′, reverse (R): 5′-GACACGTGTGGCCATTGTAG; *m*A20: F 5′-CAGTGGGAAGGGACACAACT-3′, R 5′-GCAGTGGCAGAAACTTCCTC-3′; GAPDH: F 5′-ACCCAGAAGACTGTGGATGG-3′, R 5′-CACATTGGGGGTAGGAACAC-3′; *m*NF-κB1: F 5′-CATCCCGGAGTCACGAAATC-3′, R 5′-GCACAATCTTTAGGGCCATTTT-3′; *m*NF-κB2: F 5′-CGTTCATAAACAGTATGCCATTGTG-3′, R 5′-CCCACGCTTGCGTTTCAG-3′; *m*RelB: F 5′-GCTGGGAATTGACCCCTACA-3′, R 5′-CATGTCGACCTCCTGATGGTT-3′; *m*c-Rel: F 5′-CCAGGGCAAGCTGAACCTTA-3′, R 5′-GTGGGTGATGTGGCAATCC-3′; *m*IKKγ/NEMO: F GAGTAAAGGAGGCTGGGGAG-3′, R 5′-GGAGTATTTGCAGGAGCAGC-3′; *m*TRAF2: F 5′-CATTCCTGCTCAGTGTGGTG-3′, R 5′-GTCCCAATGATGGATGCACT-3′; *m*TRAF6: F 5′-GCAAACAGCCTTTATTTGGG-3′, R 5′-AAGCCTGCATCATCAAATCC-3′; *m*RIP1: F 5′-CTCCAACACACCACTTTTGG-3′, R 5′-ACTTGCTGTCATCTAGCGGG-3′; *m*RIP2: F 5′-CAGCTGGGATGGTATCGTTT-‘3, R 5′-ACTCTGGATCCACTGTTGGG-‘3; *m*MCP-1: F 5′-AAGCCAGCTCTCTCTTCCTC-‘3, R 5′-CCTCTCTCTTTGAGCTTGGTG-‘3; *m*ICAM-1: F 5′-AAAGATCACATGGGTCGAGG-‘3, R 5′-AAAGTAGGTGGGGAGGTGCT-‘3; *m*A20: F 5′-CAGTGGGAAGGGACACAACT-‘3, R 5′-GCAGTGGCAGAAACTTCCTC-‘3.

Preparation and expression of DREAM constructs

Plasmids encoding human WT-DREAM and DNA-binding defective mutant (mut-DREAM) were custom prepared by GenScript. WT or mut-DREAM construct cloned into pCMV-SPORT6 vector was used for experiments. In DNA-binding defective mut-DREAM, alanine was substituted for arginine at 98, lysine at 101, lysine at 115, lysine at 166, lysine at 168, lysine at 178, lysine at 184, lysine at 221, and lysine at 224 (R98A-L101A-L115A-L166A-L168A-L178A-L184A-L221A-L224A). Mouse lung endothelial cells grown to ~70% confluence were transfected with WT-DREAM or mut-DREAM construct[12,41]. Plasmid DNA (1 μg/ml) was transfected using SuperFect transfection reagent (QIAGEN). At 48 h after transfection, the cells were used for experiments. WT-DREAM or mut-DREAM was ectopically expressed in HEK-293 cells. Nuclear extracts prepared from WT-DREAM or mut-DREAM expressing cells were used for electrophoretic mobility shift assay to determine DREAM binding to *h*A20 DRE4 sequence. We observed that WT-DREAM but not mut-DREAM interacted with *h*A20 DRE4 sequence.

Statistical analysis

Data were analyzed by unpaired two-tailed Student's *t* test and log-rank test. Experimental values were reported as the mean ± s.d. or mean ± s.e.m. Difference in mean values were considered significant at $p \geq 0.05$.

Supplementary Material

Refer to Web version on PubMed Central for supplementary material.

Acknowledgments

This work was supported by the National Institute of Health grant P01 HL077806. The authors wish to thank Dr. Josef M. Penninger (IMBA, Institute of Molecular Biotechnology of the Austrian Academy of Sciences, Vienna, Austria) for the DREAM knockout mice and Mr. YuBin Wu (Department of Pharmacology, University of Illinois) for help with lung endothelial cell isolation and culture.

References

1. Carrion AM, Link WA, Ledo F, Mellstrom B, Naranjo JR. Dream is a Ca^{2+}-regulated transcriptional repressor. Nature. 1999; 398:80–84. [PubMed: 10078534]
2. Carrion AM, Mellstrom B, Naranjo JR. Protein Kinase A-dependent derepression of the human prodynorphin gene via differential binding to an intragenic silencer element. Mol Cell Biol. 1998; 18:6921–6929. [PubMed: 9819380]
3. Ledo F, Carrion AM, Link WA, Mellistrom B, Naranjo JR. DREAM-αCREM interaction via leucine-charged domains derepresses downstream regulatory element-dependent transcription. Mol Cell Biol. 20:9120–9126. [PubMed: 11094064]
4. Cheng HY, et al. DREAM is a critical transcriptional repressor for pain modulation. Cell. 2002; 108:31–43. [PubMed: 11792319]
5. Iadarola MJ, Brady LS, Draisci G, Dubner R. Enhancement of dynorphin gene expression in spinal cord following experimental inflammation: stimulus specificity, behavioral parameters and opioid receptor binding. Pain. 1988; 35:313–326. [PubMed: 2906426]
6. Savignac M, et al. Transcriptional repressor DREAM regulates T-lyphocyte proliferation and cytokine gene expression. EMBO J. 2005; 24:3555–3564. [PubMed: 16177826]
7. Savignac M, et al. Increased B cell proliferation and reduced Ig production in DREAM transgenic mice. J Immunol. 2010; 185:7527–7536. [PubMed: 21059893]
8. Amir-Zilberstein L, Dikstein R. Interplay between E-box and NF-kappaB in regulation of A20 gene by DRB sensitivity-inducing factor (DSIF). J Biol Chem. 2008; 283:1317–1323. [PubMed: 17962196]
9. Hayden MS, Ghosh S. Shared Principles of NF-κB signaling. Cell. 2008; 132:344–362. [PubMed: 18267068]
10. Bonizzi G, Karin M. The two NF-κB activation pathways and their role in innate and adaptive immunity. Trends Immunol. 2004; 25:280–288. [PubMed: 15145317]
11. Hoffman A, Baltimore D. Circuitry of nuclear factor κB signaling. Immunol Rev. 2006; 210:171–186. [PubMed: 16623771]
12. Bair AM, et al. Ca^{2+} Entry via TRPC Channels is Necessary for Thrombin-Induced NF-κB Activation in Endothelial Cells Through AMP-Activated Protein Kinase and Protein Kinase Cδ. J Biol Chem. 2009; 284:563–574. [PubMed: 18990707]
13. Werner SL, et al. Encoding NF-κB temporal control in response to TNF: distinct roles for the negative regulators IκBα and A20. Genes Dev. 2008; 22:2093–2101. [PubMed: 18676814]
14. Opipari AW Jr, Hu HM, Yabkowitz R, Dixit VM. The A20 zinc finger protein protects cells from tumor necrosis factor cytotoxicity. J Biol Chem. 1992; 267:12424–12427. [PubMed: 1618749]

15. Song HY, Rothe M, Goeddel DV. The tumor necrosis factor-inducible zinc finger protein A20 interacts with TRAF1/TRAF2 and inhibits NF-κB activation. Proc Natl Acad Sci USA. 1996; 93:6721–6725. [PubMed: 8692885]
16. Wertz IE, et al. De-ubiquitination and ubiquitin ligase domains of A20 downregulate NF-κB signalling. Nature. 2004; 430:694–699. [PubMed: 15258597]
17. Boone DL, et al. The ubiquitin-modifying enzyme A20 is required for termination of Toll-like receptor responses. Nat Immunol. 2004; 10:1052–1060. [PubMed: 15334086]
18. Coornaert B, Carpentier I, Beyaert R. A20:Central gatekeeper in inflammation and immunity. J Biol Chem. 2009; 284:8217–8221. [PubMed: 19008218]
19. Hymowitz SG, Wertz IE. A20: from ubquitin editing to tumor suppression. Nat Rev Cancer. 2010; 10:332–341. [PubMed: 20383180]
20. Harhaj EW, Dixit VM. Regulation of NF-κB by deubiquitinases. Immunol Rev. 2012; 246:107–124. [PubMed: 22435550]
21. Skaug B, et al. Direct, noncatalytic mechanism of IKK inhibition by A20. Mol Cell. 2011; 44:559–571. [PubMed: 22099304]
22. Lee EG, et al. Failure to regulate TNF-induced NF-κB and cell death responses in A20-deficient mice. Science. 2000; 289:2350–2354. [PubMed: 11009421]
23. Li HL, et al. Targeted cardiac overexpression of A20 improves left ventricular performance and reduces compensatory hypertrophy after myocardial infarction. Circulation. 2007; 115:1885–1894. [PubMed: 17389268]
24. Wolfrum S, Teupser D, Tan M, Chen KY, Breslow JL. The protective effect of A20 on atherosclerosis in apolipoprotein E-deficient mice is associated with reduced expression of NF-κB target genes. Proc Natl Acad Sci U S A. 2007; 104:18601–18606. [PubMed: 18006655]
25. Haies DM, Gil J, Weibel ER. Morphometric study of rat lung cells I Numerical and dimensional characteristics of parenchymal population. Am Rev Respir Dis. 1981; 123:533–541. [PubMed: 7015935]
26. Zhao YY, et al. Endothelial cell-restricted disruption of FoxM1 impairs endothelial repair following LPS-induced vascular injury. J Clin Invest. 2006; 116:2333–2343. [PubMed: 16955137]
27. Deshmane SL, Kremlev S, Amini S, Sawaya BE. Monocyte chemoattractant protein-1 (MCP-1): An overview. J Interferon Cytokine Res. 2009; 29:313–326. [PubMed: 19441883]
28. Zhou MY, et al. *In Vivo* expression of neutrophil inhibitory factor via gene transfer prevents LPS-induced lung neutrophil infiltration and injury by β_2 integrin-dependent mechanism. J Clin Invest. 1998; 101:2427–2437. [PubMed: 9616214]
29. Broman MT, et al. Cdc42 regulates adherens junction stability and endothelial permeability by inducing α-catenin interaction with the vascular endothelial cadherin complex. Circ Res. 2006; 98:73–80. [PubMed: 16322481]
30. Sato S, et al. Essential function for the kinase TAK1 in innate and adaptive immune responses. Nat Immunol. 2005; 6:1087–1095. [PubMed: 16186825]
31. Ye X, et al. Divergent roles of endothelial NF-κB in multiple organ injury and bacterial clearance in mouse models of sepsis. J Exp Med. 2008; 205:1303–1315. [PubMed: 18474628]
32. Ghosh S, Hayden MS. New regulators of NF-κB in inflammation. Nat Immunol Rev. 2008; 8:837–848.
33. Yin X, Krikorian P, Logan T. Induction of RIP-2 kinase by proinflammatory cytokines is mediated via NF-κB signaling pathways and involves a novel feed-forward regulatory mechanism. Mol Cell Biochem. 2010; 333:251–259. [PubMed: 19693652]
34. Sakurai H. Targeting of TAK1 in inflammatory disorders and cancer. Trends Pharmacol Sci. 2012; 33:522–530. [PubMed: 22795313]
35. Rey S, et al. Synergistic effect of HIF-1alpha gene therapy and HIF-1-activated bone marrow-derived angiogenic cells in a mouse model of limb ischemia. Proc Natl Acad Sci U S A. 2009; 106:20399–20404. [PubMed: 19948968]
36. Hickey MJ, et al. Inducible nitric oxide synthase (iNOS) in endotoxemia: chimeric mice reveal different cellular sources in various tissues. FASEB J. 2002; 16:1141–1143. [PubMed: 12039841]

37. Vogel SM, et al. Abrogation of thrombin-induced increase in pulmonary microvascular permeability in proteinase activated receptor-1(PAR-1$^{-/-}$) knockout mice. Physiol Genomics. 2000; 4:137–145. [PubMed: 11120874]

38. Tiruppathi C, et al. Impairment of store-operated Ca^{2+} entry in TRPC4$^{-/-}$ mice interferes with increase in lung microvascular permeability. Circ Res. 2002; 91:70–76. [PubMed: 12114324]

39. Wang YL, et al. Innate immune function of the aherens junction protein p120-catenin in endothelial response to endotoxin. J Immunol. 2011; 186:3180–3187. [PubMed: 21278343]

40. Rittirsch D, Huber-Lang MS, Flierl MA, Ward PA. Immuno design of experimental sepsis by cecal ligation and puncture. Nat Protoc. 2009; 4:31–36. [PubMed: 19131954]

41. Paria BC, et al. Ca^{2+} influx-induced by PAR-1 activates a feed forward mechanism of TRPC1 expression via NF-κB activation in endothelial cells. J Biol Chem. 2006; 281:20715–20727. [PubMed: 16709572]

42. Gatta R, Mantovani R. Single nucleosome ChIPs identify an extensive switch of acetyl marks on cell cycle promoters. Cell Cycle. 2010; 9:2149–59. [PubMed: 20505338]

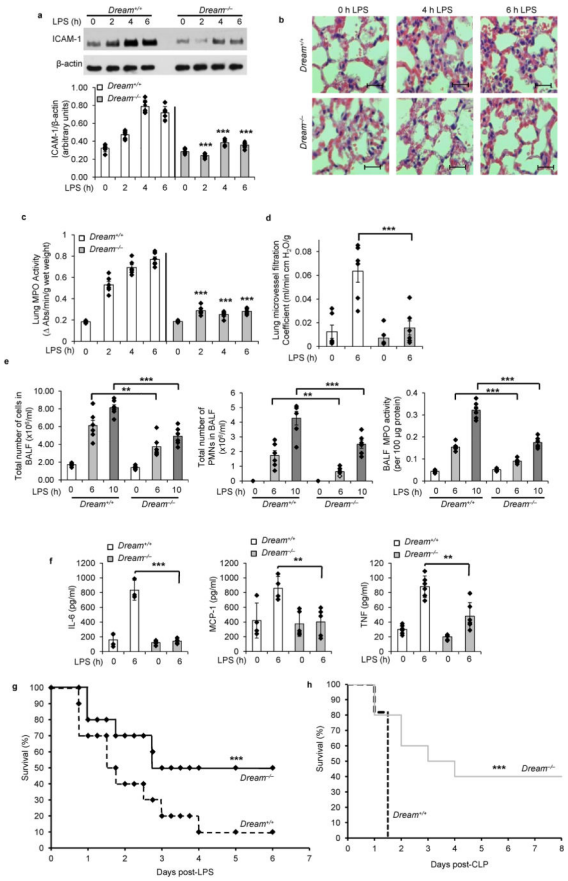

Figure 1. Genetic deletion of DREAM prevents endotoxin-induced lung inflammatory injury and sepsis-induced mortality

Dream$^{+/+}$ and *Dream*$^{-/-}$ mice (n = 6 per group) were challenged with LPS (10 mg/kg, i.p.) and lungs were removed at the indicated times. **a**, ICAM-1 protein expression in lungs was determined by immunoblot (IB). Immunoblots from 6 experiments were quantified and values normalized to β-actin (bottom panel). **b**, Haematoxylin and eosin staining of lung sections (bar = 100 μm). **c,** Reduction in lung tissue MPO activity in *Dream*$^{-/-}$ mice. **d**, Pulmonary microvessel filtration coefficient ($K_{f,c}$) determined in lungs from *Dream*+/+ and *Dream*$^{-/-}$ mice. **e,** After LPS challenge, inflammatory cells present in BALF was measured. Total number of PMNs (middle panel) and MPO activity (right panel) in BALF. **f**, Cytokines (IL-6, MCP-1, and TNF) in BALF were measured. **p< 0.01, ***p<0.001, different from LPS-injected *Dream*$^{-/-}$ mice. Data are representative of six experiments (**a, f**; mean ± s.d.; **c,d,e**, mean ± s.e.m; unpaired two-tailed Student's *t*-test). **g,** Survival of *Dream*$^{+/+}$ and *Dream*$^{-/-}$ mice after LPS challenge (10 mg/kg, i.p.). Age and weight matched male *Dream*$^{+/+}$ and *Dream*$^{-/-}$ mice were followed for 12 days after LPS administration (there was no mortality after day 6 in both groups). n = 20 in each group. ***p< 0.001, vs. *Dream*$^{+/+}$ mice using the log-rank test. **h,** Survival after CLP. Age and weight matched male *Dream*$^{+/+}$ and *Dream*$^{-/-}$ mice were challenged with CLP and observed for two weeks. n = 12 in each group. ***p< 0.001, vs. *Dream*$^{+/+}$ mice using the log-rank test.

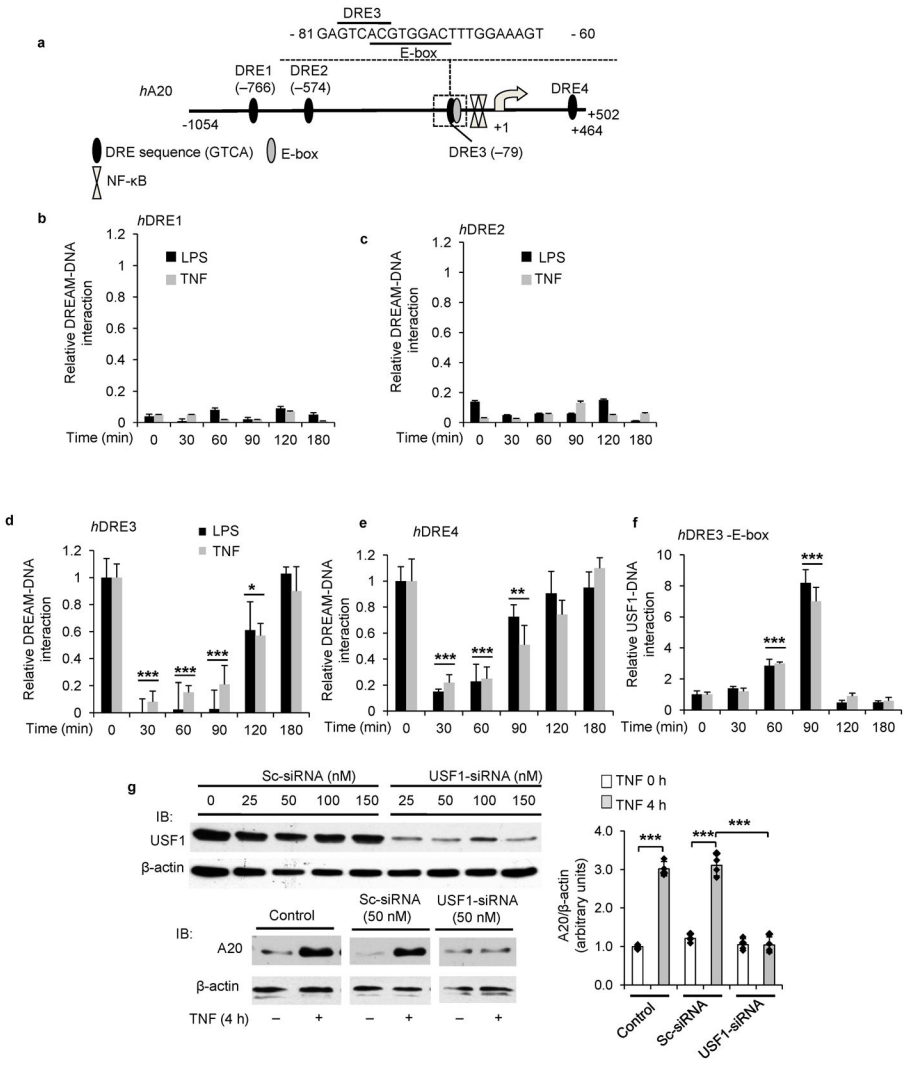

Figure 2. DREAM and USF1 coordinate A20 transcription

a, DREAM binding DRE elements and other transcription factors binding sites in human (*h*) A20 gene. *h*A20 gene contains 4 DRE elements. DRE3 overlaps with E-box sequence. **b–e**, CHIP assay used to assess interaction of DREAM with *h*A20 gene DREs in HLMVECs. HLMVECs challenged with LPS (1 μg/ml) or TNF (500 units/ml) for indicated times. Data are pooled from four experiments (mean ± s.d.). LPS or TNF challenge produced similar responses. **d**, ***p< 0.001, control cells (0 min) vs. 30, 60 or 90 min; *p< 0.05, 0 vs. 120 min. **e**, ***p< 0.001, 0 min vs. 30 or 60 min; **p< 0.01, 0 vs. 90 min (unpaired two-tailed Student's *t*-test). **f,** LPS- or TNF-induced association and dissociation of USF1 with DRE3 element was determined by CHIP. Data are from four experiments (mean ± s.d.). ***p< 0.001, 0 vs. 60 min; ***p< 0.001, 0 vs. 90 min (unpaired two-tailed Student's *t*-test). **g,** USF1 knockdown suppressed A20 expression in endothelial cells. HUVECs transfected with control Sc-siRNA or USF1-siRNA (*top panels*) were used to determine USF1 protein expression (*top panels*) or A20 protein induction in response to TNF (*bottom panels*). Data are representative of three experiments. Immunoblots were quantified and values (mean ± s.e.m) normalized to β-actin (*right panel*). ***p< 0.001, control vs. TNF stimulated; *p<

0.001, Sc-siRNRA treated vs. USF1-siRNA treated (unpaired two-tailed Student's *t*-test). **b–e**, DREAM binding to DRE sites was normalized to input and then LPS- or TNF-induced DREAM association or dissociation with DRE sites was expressed relative to basal values. **f**, in response to LPS or TNF challenge, USF1 binding fold-increase over basal with *h*DRE3 was shown.

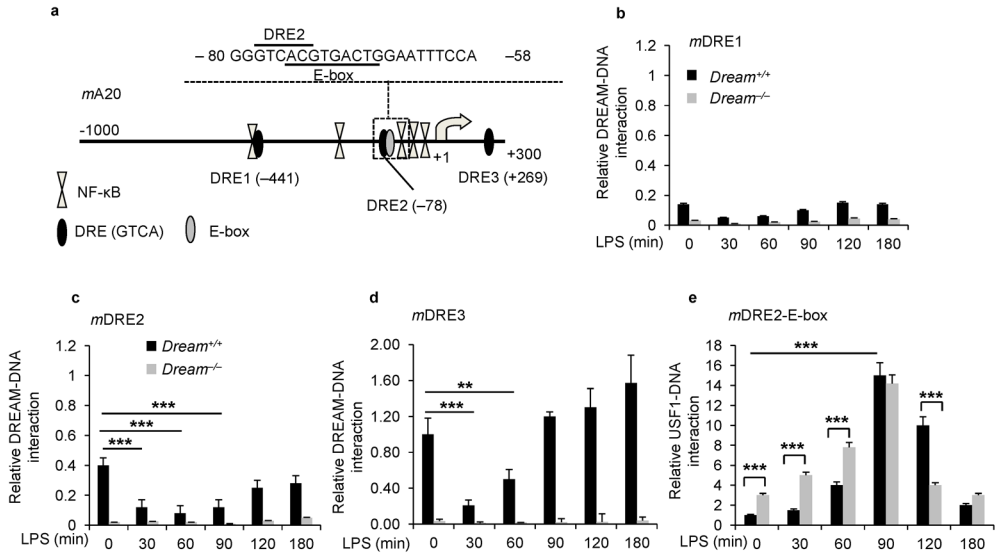

Figure 3. Analysis of DREAM and USF1 regulation of A20 transcription in Dream$^{-/-}$ mice

a, Representation of DREAM binding DRE elements and other transcription factors binding sites in mouse (*m*) A20 gene. DRE2 sequence overlaps with E-box sequence in *m*A20 promoter. **b–d,** BMDMs from *Dream*$^{+/+}$ or *Dream*$^{-/-}$ mice challenged with LPS (1 μg/ml) for indicated time periods were used for CHIP assay. Results are from four experiments (mean ± s.d.). No significant DREAM binding observed in *Dream*$^{-/-}$ BMDMs. **c**, ***p< 0.001, control cells (0 min) vs. 30, 60 or 90 min in *Dream*$^{+/+}$ BMDMs. **d**, ***p< 0.001, 0 min vs. 30, or 60 in *Dream*$^{+/+}$ BMDMs. **e**, BMDMs from *Dream*$^{+/+}$ or *Dream*$^{-/-}$ mice challenged with LPS (1 μg/ml) for indicated times were used for CHIP assay to determine USF1 binding to DRE2. Results are from four experiments (mean ± s.d.). ***p< 0.001, 0 vs. 30, 60, or 90 min either *Dream*$^{+/+}$ or *Dream*$^{-/-}$. ***p< 0.001, *Dream*$^{+/+}$ vs. *Dream*$^{-/-}$ at 0, 30, 60, or 120 min (unpaired two-tailed Student's *t*-test). **b–d**, DREAM binding to DRE sites was normalized to input and then LPS-induced DREAM association or dissociation with DRE sites was expressed relative to basal values. **e**, in response to LPS challenge, USF1 binding fold-increase over basal with *m*DRE2 was shown.

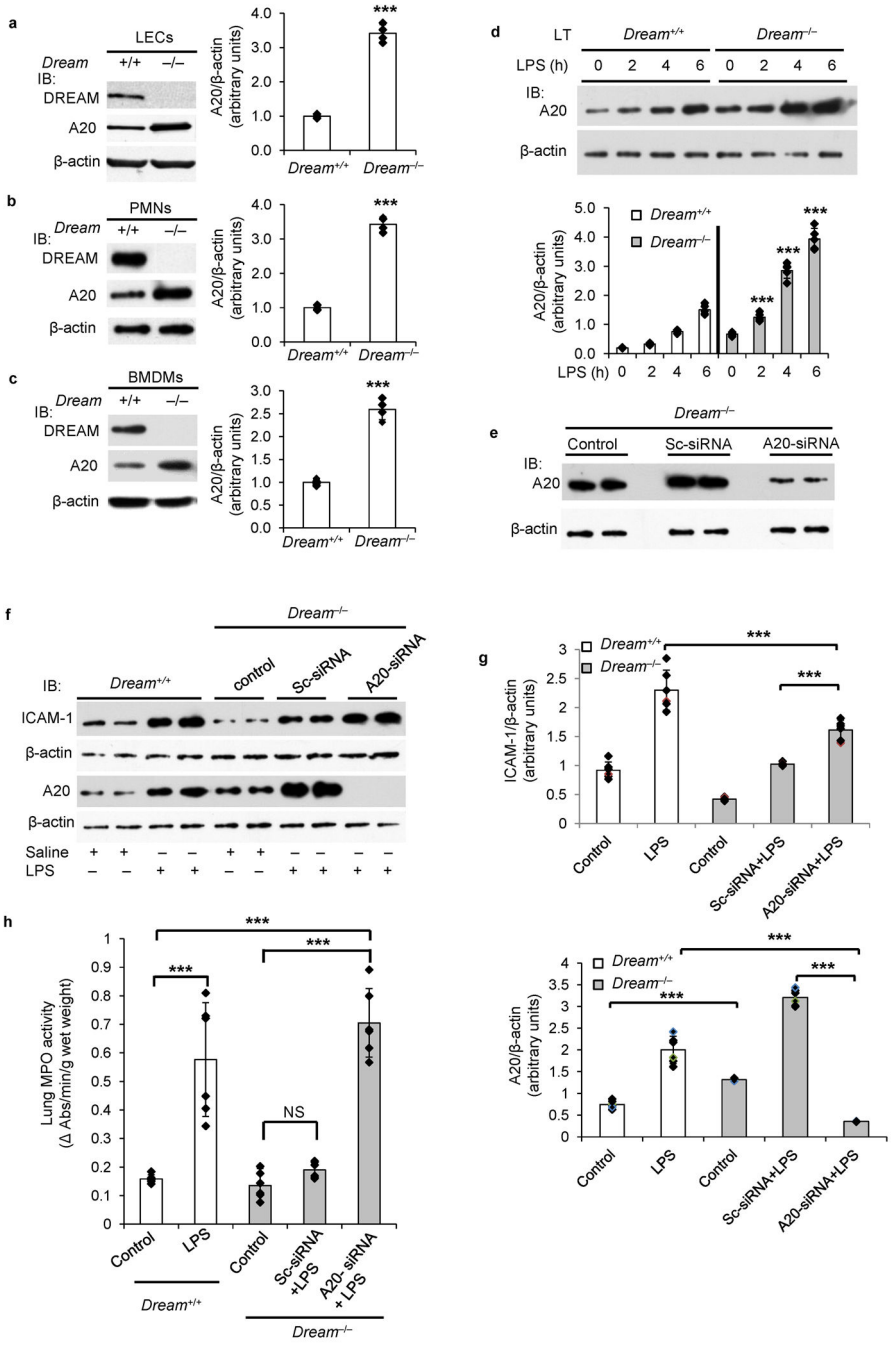

Figure 4. DREAM deficiency in mice augments basal and induced A20 expression

a–c, Immunoblots showing DREAM expression in LECs (**a**), PMNs (**b**), and BMDMs (**c**) from WT (*Dream*$^{+/+}$) and *Dream*$^{-/-}$ mice. Data are representative of four experiments. A20 expression was calculated from the A20-to-β-actin ratio (*right panels*). ***p<0.001 (unpaired two-tailed Student's *t*-test). **d**, LPS induced A20 expression is augmented in lungs of *Dream*$^{-/-}$ mice. *Dream*$^{+/+}$ and *Dream*$^{-/-}$ mice were challenged with LPS (10 mg/kg, i.p.) and lungs were removed at the indicated times as described in Fig. 1a. Lung tissue (LT) was used for IB analysis of A20 protein expression. n = 5 per time point in each group.

Results shown are mean ± s.e.m. ***p< 0.001 (unpaired two-tailed Student's *t*-test), different from *Dream*$^{+/+}$ mice. **e–h,** A20 knockdown restores LPS-induced lung inflammatory injury in *Dream*$^{-/-}$ mice. *Dream*$^{-/-}$ mice were injected with saline, Sc-siRNA, or A20-siRNA. At 48 h after injection, lungs harvested were used to determine A20 protein expression by IB (**e**). At 48 h after injection with saline, Sc-siRNA, or A20-siRNA injected *Dream*$^{-/-}$ mice were challenged with saline or LPS (10 mg/kg, i.p.). At 6 h after saline or LPS challenge, lungs harvested were used to determine ICAM-1 and A20 expression by IB (**f** and **g**) or MPO activity (**h**). In this experiment, *Dream*$^{+/+}$ mice were also used as a positive control to study the LPS effect. Data are representative of six experiments. N= 6 in each group; Values are mean ± s.e.m. ***p< 0.001 (unpaired two-tailed Student's *t*-test), different from respective control groups.

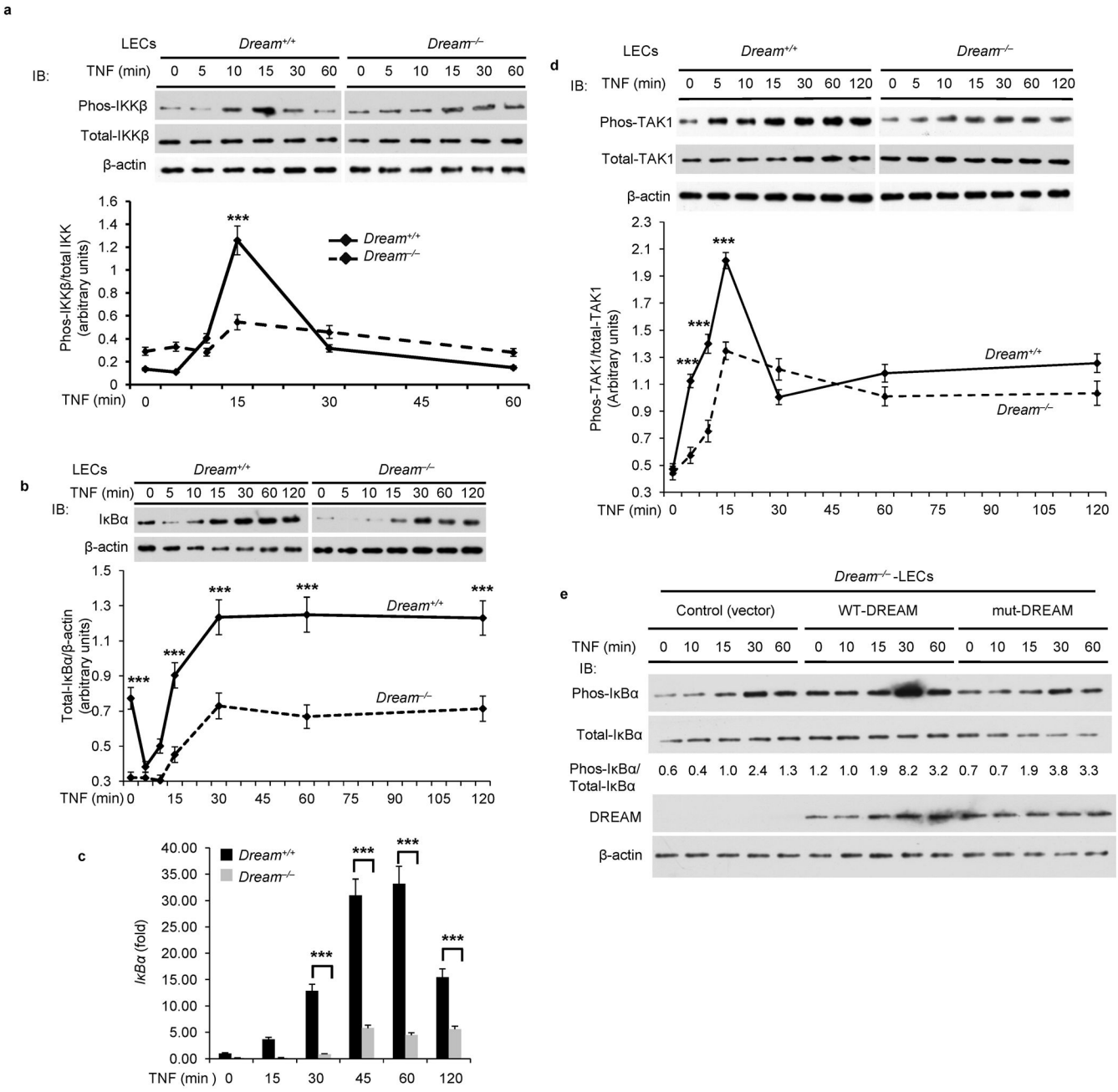

Figure 5. DREAM deletion attenuates TNF-induced TAK1 and IKK activation in lung endothelial cells

a, *Dream*$^{+/+}$ or *Dream*$^{-/-}$ LECs treated with TNF (1000 U/ml) for different time intervals were used to measure IKKβ phosphorylation. *Top*, representative immunoblots (IBs) from four experiments. *Bottom*, the ratio of phospho-IKKβ to total-IKKβ. **b,** *Top panel:* TNF-induced IκBα protein expression was measured in LECs from *Dream*$^{+/+}$ and *Dream*$^{-/-}$ mice. **c,** Quantitative RT-PCR was used to determine TNF-induced IκBα mRNA expression in LECs from *Dream*$^{+/+}$ or *Dream*$^{-/-}$ mice. **d**, *Dream*$^{+/+}$ or *Dream*$^{-/-}$ LECs treated with TNF (1000 U/ml) for different time intervals were used to measure TAK1 phosphorylation

at Thr-184/187. *Top*, representative IBs from four experiments. *Bottom*, quantitative results, the band intensity measured by densitometry and the ratio of phospho-TAK1 to total TAK1 was calculated. In **a–d**, results are mean ± s.d. of 4 experiments. ***p<0.001 (unpaired two-tailed Student's *t*-test). **e**, *Dream*$^{-/-}$ LECs were transfected with vector, WT-DREAM, or DNA-binding defective mutant (mut-DREAM). At 48 h after transfection, cells exposed to TNF were immunoblotted with anti-phopho-IκBα, anti-IκBα, anti-DREAM, or anti-β-actin. Representative IBs from two separate experiments are shown. *In the middle*, the ratio of phopho-IκBα to total IκBα is shown. **f** and **g,** *top panels:*

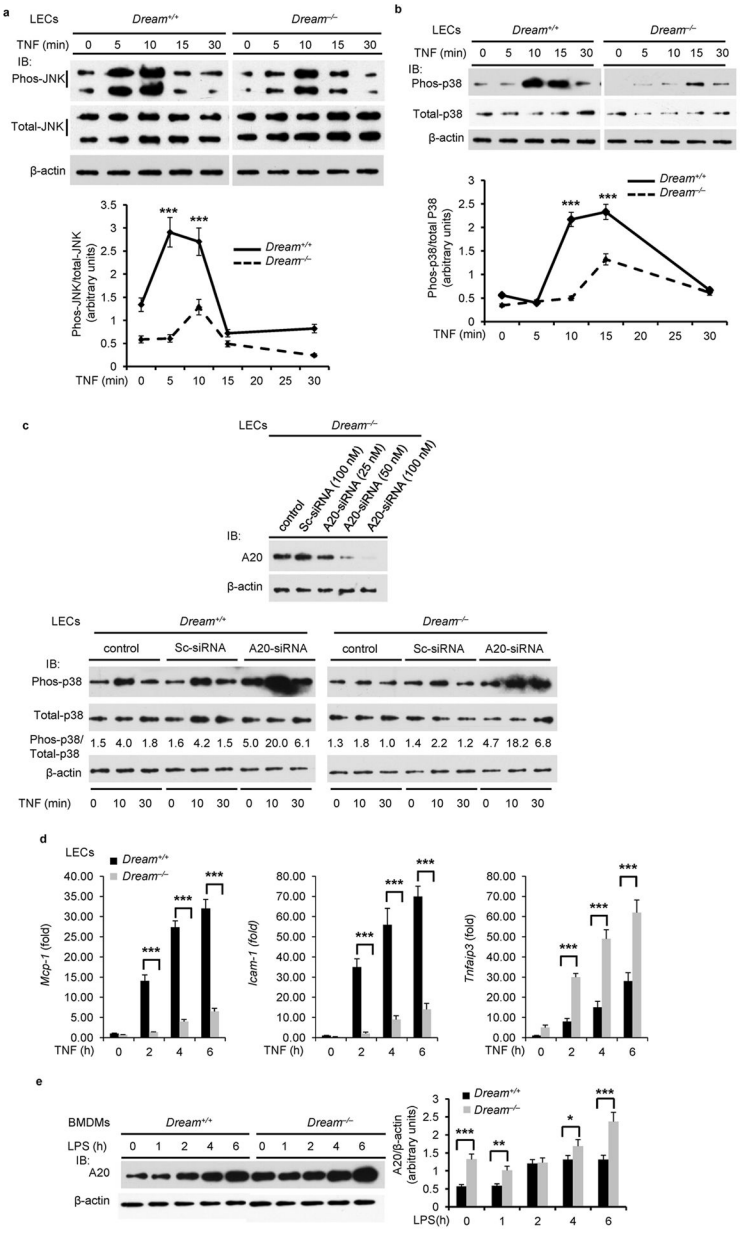

Figure 6. DREAM deletion attenuates TNF-induced JNK and p38 MAPK activation in lung endothelial cells

TNF-induced phosphorylation of JNK (**a**) or p38 (**b**) was measured in LECs from *Dream*$^{+/+}$ and *Dream*$^{-/-}$ mice. *Bottom panels*, the ratio of phospho-JNK to total-JNK or phospho-p38 to total-p38. In **a, b,** results are mean ± s.d.; ***p< 0.001 (unpaired two-tailed Student's *t*-test). **c**, LECs from WT or *Dream*$^{-/-}$ mice were transfected with Sc-siRNA or A20-siRNA. At 48 h after transfection, cells were used to measure A20 protein expression (*top*) or p38 phosphorylation after stimulation with TNF (*bottom*). Results shown are representative of three experiments. The ratio of phopho-p38 to total-p38 is indicated. **d,** *Dream*$^{+/+}$ or *Dream*$^{-/-}$ LECs treated with TNF (1000 U/ml) for different time intervals were used to determine mRNA expression for MCP-1, ICAM-1, and A20 by qRT-PCR. Results shown

are mean ± s.e.m. of 4 experiments. ***p<0.001(unpaired two-tailed Student's *t*-test). **e**, BMDMs in culture from *Dream*$^{+/+}$ and *Dream*$^{-/-}$ mice exposed to LPS (100 ng/ml) for different time intervals were used to determine A20 protein expression. Data shown are representative of three experiments. Immunoblots were quantified (*right panel*). *p<0.05; **p<0.01; ***p<0.001 (unpaired two-tailed Student's *t*-test).

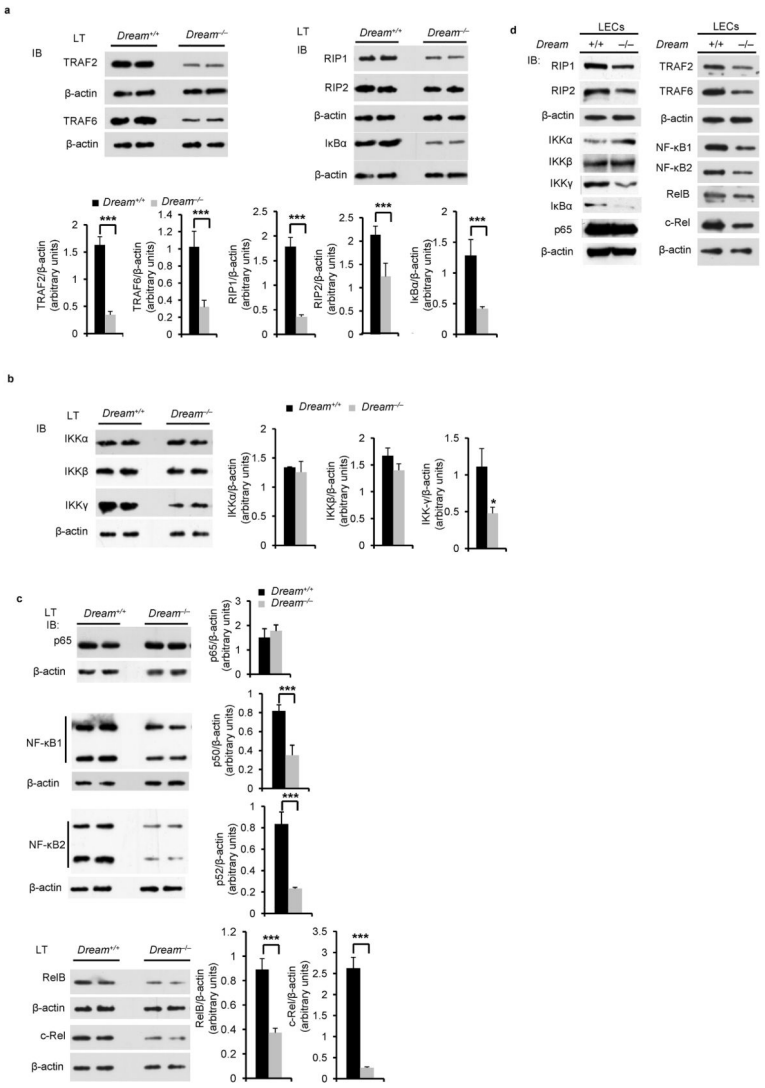

Figure 7. DREAM differentially regulates the expression of NF-κB signaling components and target genes

Lung tissue (LT) from *Dream*$^{+/+}$ and *Dream*$^{-/-}$ mice was used to determine the expression of TRAFs (TRAF2 and TRAF6), RIPs (RIP1 and RIP2), and IκBα (**a)**, IKKs (IKKα, IKKβ, IKKγ) (**b**), and NF-κB proteins (p65/RelA, NF-κB1/p50, NF-κB2/p52, RelB, and c-Rel) (**c**). Representative IBs are shown in **a–c**. Quantitative comparisons between *Dream*$^{+/+}$ and *Dream*$^{-/-}$ are shown. n = 5 mice per group (mean ± s.d.). ***p<0.001 (unpaired two-tailed Student's *t*-test). In **d**, LECs from *Dream*$^{+/+}$ and *Dream*$^{-/-}$ mice were used for immunoblot analysis to determine the expression of NF-κB signaling components as above. Results are representative of three experiments.

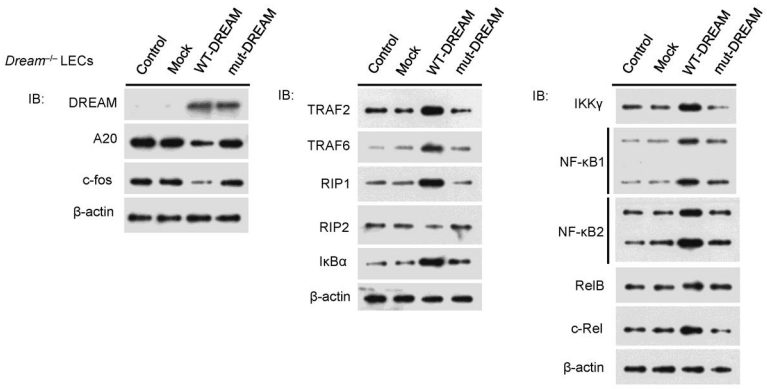

Figure 8. WT-DREAM expression restores NF-κB signaling components level in DREAM deficient LECs

Dream$^{-/-}$ LECs were transfected with empty vector (mock), WT-DREAM, or mut-DREAM (DNA-binding defective mutant). At 48 h after transfection, cells were used for IB analysis. Results are representative of at least two independent experiments.